

High Contrast Imaging Testbed for the Terrestrial Planet Finder Coronagraph

Andrew E. Lowman*, John T. Trauger, Brian Gordon, Joseph J. Green,
Dwight Moody, Albert F. Niessner, Fang Shi

Jet Propulsion Laboratory (JPL), California Institute of Technology

ABSTRACT

The Terrestrial Planet Finder (TPF) mission is planning to launch a visible coronagraphic space telescope in 2014. To achieve TPF science goals, the coronagraph must have extreme levels of wavefront correction (less than 1 Å rms over controllable spatial frequencies) and stability to get the necessary suppression of diffracted starlight ($\sim 10^{-10}$ contrast at an angular separation $\sim 4 \lambda/D$). TPF Coronagraph's primary platform for experimentation is the High Contrast Imaging Testbed, which will provide laboratory validation of key technologies as well as demonstration of a flight-traceable approach to implementation. Precision wavefront control in the testbed is provided by a high actuator density deformable mirror. Diffracted light control is achieved through use of occulting or apodizing masks and stops. Contrast measurements will establish the technical feasibility of TPF requirements, while model and error budget validation will demonstrate implementation viability. This paper describes the current testbed design, development approach, and recent experimental results.

Keywords: TPF, coronagraph, wavefront sensing, active optics, deformable mirror

1. INTRODUCTION

Terrestrial Planet Finder (TPF) will detect and characterize earth-like planets around nearby stars.¹ TPF Coronagraph is currently in its formulation phase, developing needed technology and performing design trades for a mission.² Current thinking has a coronagraph mission launching in the 2014 timeframe, with a stellar interferometer launch several years later. The coronagraph will detect visible light from the parent star that is reflected by a planet, while the interferometer will measure infrared light radiated by the planet. For either architecture, the requirements are challenging.

The driving requirement for a coronagraph is high contrast at a small angular separation. Contrast of 10^{-9} or 10^{-10} is necessary, while the contrast stability must be 10^{-11} . For nearby stars, the angular separation between the star and planet will be $3-5 \lambda/D$, where λ is the wavelength and D is the largest dimension of the telescope's likely elliptical primary mirror; this number depends on the exact value of D selected based on telescope observing efficiency and launch vehicle packaging considerations. To achieve these requirements, a coronagraph requires several key features: extreme levels of wavefront sensing and control; high performance occulting masks and stops; stray light suppression; a highly stable optomechanical system; uniform coatings; minimal polarization effects; and accurate diffraction models to allow simulation of these issues and predictions of on-orbit performance. TPF has built the High Contrast Imaging Testbed (HCIT) to validate these critical technologies and to demonstrate implementation readiness for a coronagraph space mission.

* Contact: Andrew.E.Lowman@jpl.nasa.gov; phone 1 818 354 0526; Jet Propulsion Laboratory, M/S 306-451, 4800 Oak Grove Dr, Pasadena, CA, USA 91109-8099

2. TESTBED DESCRIPTION

The HCIT consists of an optical experiment inside a vacuum chamber. Commercial off-the-shelf (COTS) components were used where possible to expedite construction of the testbed while keeping costs reasonable. These may be replaced with custom parts over time as needed to improve performance.

1. Optical Layout

The bench is a 5' by 7' COTS vibration-damped optical table. Semi-custom optics are held by vacuum-compatible COTS optical mounts; COTS motorized translation stages support semi-custom cameras. Custom risers and standoffs are used to get the components to a common beam height. The current system is a classical Lyot coronagraph; the layout is shown in Figure 1.

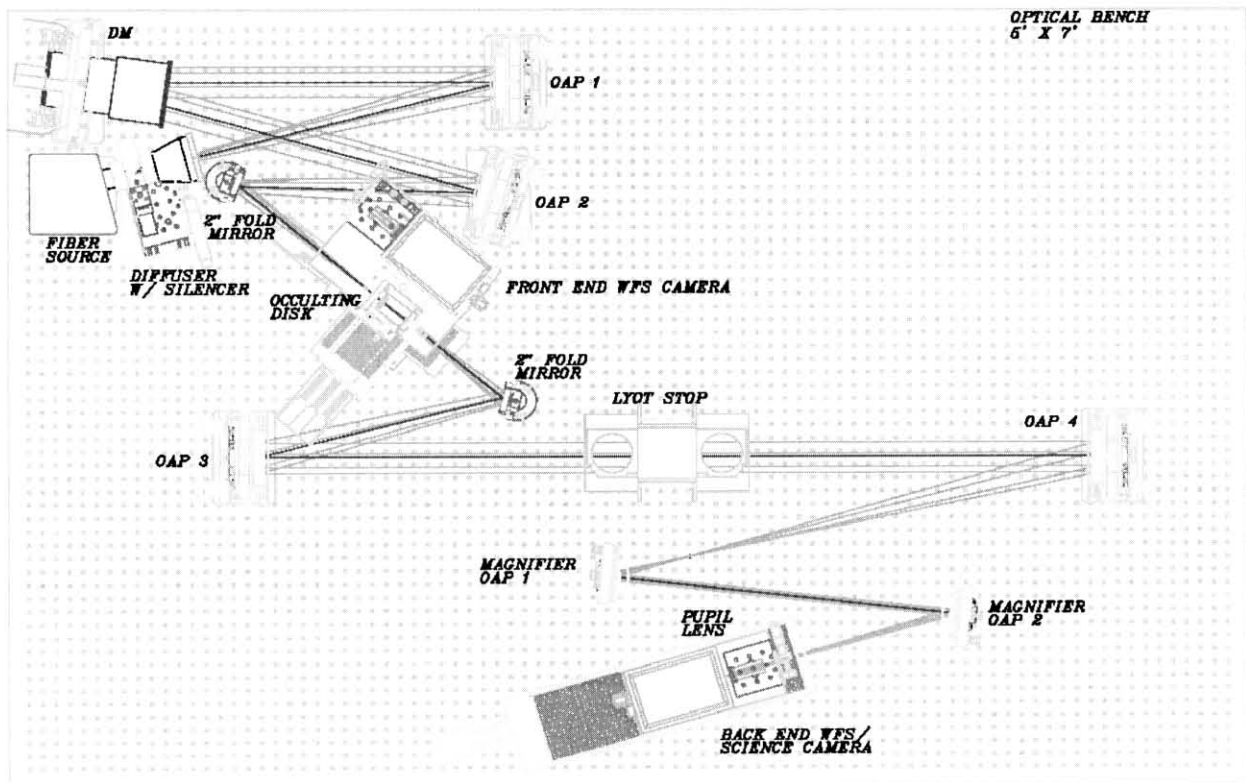


Figure 1. Current Testbed Layout

A star source is simulated by a five micron pinhole illuminated by a fiber, which is fed from a source outside the chamber. The beam is collimated by an off-axis parabolic mirror (OAP) and directed to a high-density deformable mirror (DM). The reflected beam is focused by a second OAP. An occulting mask at that location attenuates light from the [simulated] star while minimally affected the light from any planet(s) near the star. The transmitted beam is collimated by a third OAP and propagated to a pupil plane, conjugate to the DM, where residual light from the star will be concentrated in a ring near the outside of the pupil. This light is blocked by an undersized Lyot stop, which will pass most of the light from any planet(s). The remaining light is focused by a fourth OAP. A field stop is located at this focus, to assist in blocking stray light. To get Nyquist or better sampling on the science camera, a pair of smaller OAPs is used to magnify the image.

The cameras use low-noise science grade CCDs. Two cameras are available; the rear camera, used for science measurements, has 13 micron pixels. A second camera, with 7.5 micron pixels, is selectable at the first (occulting mask) focus. Both cameras are mounted on translation stages, to permit through focus wavefront sensing. A diffuser source is selectable near the pinhole, to provide a uniform background for flat fielding of the cameras and easier alignment of the occulting masks. Additional stages are used to insert pupil imaging lenses in front of either camera.

Coating properties are important to achieving high contrast. Bare gold coatings are currently used on all mirrors to minimize polarization effects. Polarization due to the testbed optical design and coatings will be analyzed. When the optics are recoated to improve performance, other coating materials will be considered, and the uniformity of the coatings will be measured.

Photographs of the bench are shown in Figure 2. The two tallest (black) objects are the thermoelectric coolers on top of the cameras; the other tall black object is the current mechanism used for Lyot stops. The DM is located in the lower left corner of Figure 2a; at the time this photograph was taken, we were awaiting delivery of a DM and had a flat mirror installed in its place. A custom Michelson interferometer (not shown), used for testing and calibrating DMs, is installed in the chamber below the HCIT bench.

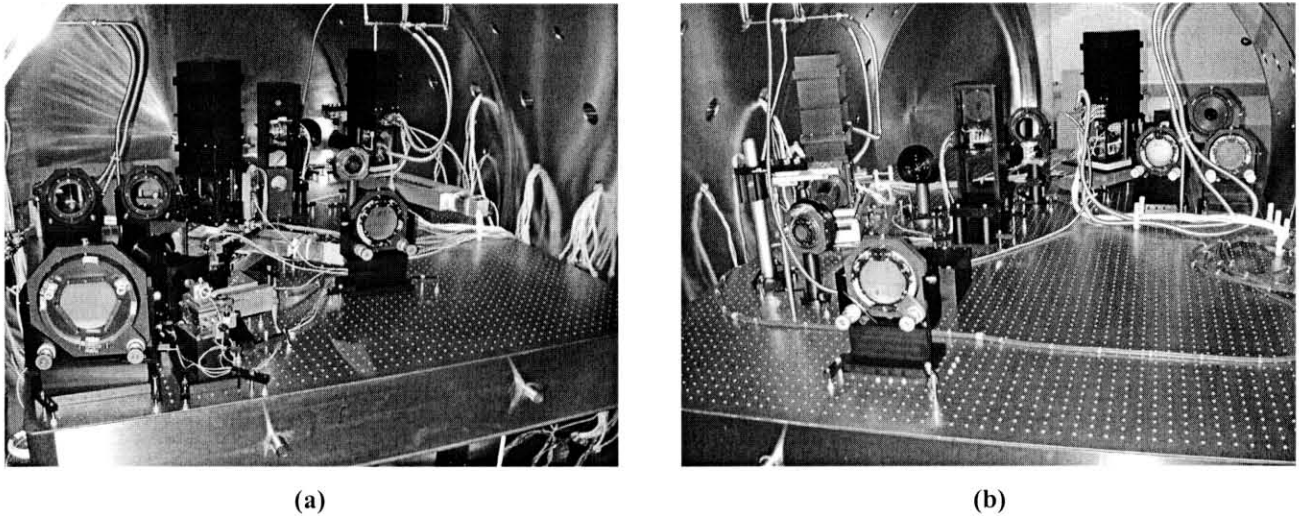


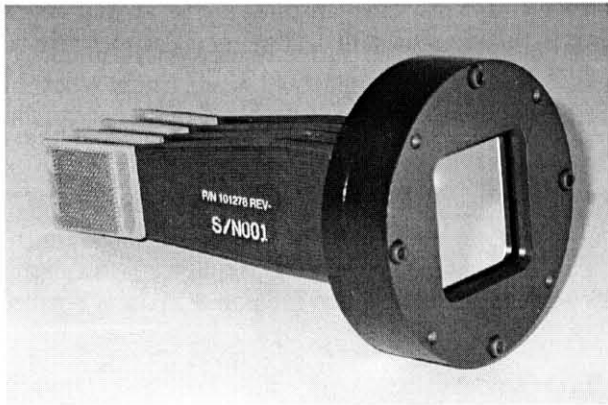
Figure 2. Testbed Views: (a) Front; (b) Back

2. Illumination

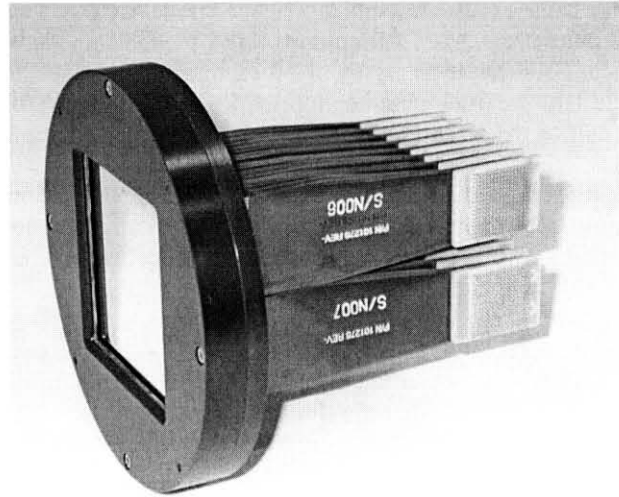
An external source module provides both a broadband and laser source. The white light source is a Xenon lamp combined with neutral density and spectral filters and imaged onto a fiber. The laser is currently a 785 nm fiber-coupled laser diode. The source is selected by connecting the appropriate fiber to the chamber's input fiber.

3. Wavefront Sensing and Control System

The enabling technology for a space coronagraph mission is a high-density deformable mirror. Such DMs have been under development for several years at Xinetics, Inc.³ A 1024-actuator DM (32x32 array) is currently operating in the HCIT. A 4096-actuator DM (64x64 array) will be tested with our Michelson interferometer and installed in the testbed in the near future. These mirrors are pictured in Figure 4. The DM enables wavefront control at sub-Å precision, an unprecedented level. The mirrors have a stroke on the order of 500 nm, with an actuator pitch of 1 mm. The mirrors are driven by custom high voltage ASICs located in vacuum; the controller is a compact 4096-channel Xinetics-built multiplexer that resides outside the chamber. These electronics enable 16-bit control of the DM; our earlier rack-sized multiplexer had only 12-bits of precision and proved to be the limiting error source for contrast.



(a)



(b)

Figure 3. Deformable Mirrors: (a) 1024 Actuators; (b) 4096 Actuators

Wavefront sensing measurements may be made at either the front or back cameras in the testbed. The “front-end” technique uses phase retrieval in a manner similar to what is under development for JWST. The specific approach we use is a modified Gerchberg-Saxton (MGS) algorithm; this iterative Fourier transform method extracts the wavefront from a series of through-focus images and a pupil image.^{4,5} The resulting wavefront is used to calculate a control for the DM. There are several errors that will limit this approach: the front camera has small pixels, which introduce blurring due to inter-pixel crosstalk; there is a systematic difference due to non-common path optics, since the camera window is not in the coronagraph path and the occulting mask is not in the camera path; with the 4096-actuator DM, the image will be undersampled by this camera. Consequently, achievable contrast is limited to $\sim 10^{-6}$ using this method. The MGS approach is still useful for calibrating the DM, as well as putting the system into a relatively well-corrected state prior to engaging more advanced algorithms using the back camera.

Ultimate performance will be achieved using images taken with the back camera. These “back-end” approaches operate directly on images taken through the occulting mask and Lyot stop. One algorithm under investigation uses pupil images; our current algorithm assumes a uniform amplitude, but improved algorithms may overcome this limitation.⁶ Our best results to date have been achieved using a speckle nulling algorithm that operates directly on coronagraphic images.⁷ This approach attempts to quash individual speckles in the image by dithering the DM. The algorithm targets a specific speckle by applying a sine wave on the DM (pupil) associated with that particular spatial frequency. The intensity of the speckle is measured as the phase of the sine wave is changed, and the DM is then set to minimize that intensity.

One advantage of the back-end coronagraphic image approach is the ability to compensate for amplitude errors. The system has a low frequency amplitude error due to the uniformity of the input beam; higher frequency errors are also present and their source is under investigation. These errors are significant; if the DM is set to zero out phase errors, contrast will not get below 10^{-7} , if that. Using a “half-hole” algorithm, performance in one half of the image plane may be improved at the expense of the other.

To achieve highest contrast on both halves of the image plane, a second DM is necessary to correct for amplitude errors. Our current optical layout does not have adequate clearance for an additional DM, but a redesign is planned to support this. Wavefront sensing algorithm development is also needed to separate the effects of amplitude and phase errors. Another approach that uses two DMs is under development at NASA/Goddard Space Flight Center and may be tested in the HCIT.⁸

4. Diffractive Light Suppression

The HCIT is currently configured as a Lyot coronagraph. Our baseline occulting masks use patterns written on high energy beam sensitive (HEBS) glass. The peak optical density occurs at 800 nm, but there is a strong variation with wavelength.⁹ Wider bandwidth HEBS glass has been developed by Canyon Materials, Inc. and is undergoing testing. Our current Lyot stops are simple blackened sheet metal with a sharp edge. TPF is exploring other approaches to masks and stops, mostly through industrial and university partners, as well as developing instrumentation to characterize both the amplitude and phase properties of these components. The HCIT may be easily configured as an apodized coronagraph, by simply replacing the Lyot stop with an apodized stop (such as a Spergel mask¹⁰) and placing a blocking disk at the downstream focus. In this arrangement, the occulting mask at the first focus is not used.

The background level must be minimized to achieve high contrast. The enclosed chamber prevents external sources from affecting our measurements, and read noise is only a few electrons in our science-grade camera. However, a potential limiting factor is stray light in the testbed. Reflection off the pinhole may allow returning light (especially light reflected off the CCD) to re-enter the system. Scattering due to optical surface roughness and contamination is another concern. Simple baffles and a field stop have been implemented; however, as is often the case in stray light suppression, some of these components could conceivably make the situation worse. A stray light analysis will be conducted to predict ultimate system performance; scrutinize current baffles and design improved ones as needed; impose requirements on improved optics; and establish a required level for contamination when the optics are recoated or replaced.

5. Facility

Figure 4 is an external photograph of the testbed. The racks contain the source module; electronics to control the DM, stages, and cameras; and computers used to control the testbed hardware and support instrumentation.

The HCIT chamber is pumped to 10^{-3} Torr, sufficient to provide a stable and dark environment for experiments while eliminating atmospheric effects. The testbed is heavily instrumented with temperature sensors, as well as a few accelerometers, with contamination monitors planned for the future. The chamber wall temperature is maintained to ± 0.1 K using a simple control system. More sophisticated control is used to stabilize the DM temperature to milli-K levels. These electronics may also be used to drive heaters on other optical components, mounts, and the testbed bench.



Figure 4. Testbed Facility

3. MODELING AND HARDWARE DEVELOPMENT APPROACH

The initial testbed construction predated the formal organization of TPF Coronagraph and followed years of coronagraph modeling and DM development. The current optical layout is based on an existing coronagraph design, packaged to fit inside a moderately-sized vacuum chamber. The testbed was assembled with a standard vacuum-compatible optical table, COTS mounts, and semi-custom mirrors ($\lambda/20$ PV) aligned inside a clean tent in an ordinary laboratory. To date, work has focused on rapidly obtaining high contrast, with experimental data compared to models and used to identify the dominant error sources and provide guidance for near-term improvements to the system. This type of experimentation will continue and is expected to improve the contrast and identify error sources.

In parallel, longer term development will proceed using a more flight traceable approach. The system was built without an error budget, and component characterization and calibration activities were limited in the interests of schedule. An error budget is under development and will be used to drive the requirements for improvements to the hardware. Characterization and calibration of the components will be improved as changes are made to the system, and as-built parameters for the system will be derived. This approach emphasizes model and error budget validation rather than contrast improvement; if experimental results do not match predictions, effort will be directed to understanding the discrepancy. Contrast improvements will come by replacing the limiting components, as guided by the error budget. The testbed will also be used to validate TPF error budgets, models, and modeling tools, to increase confidence on predictions made for the TPF design that cannot be readily investigated in the lab.

4. RESULTS

After alignment and initial experimentation in the clean tent, the bench was moved into the chamber in April 2003. Prior to delivery of a first fully-functional DM, experiments were conducted to establish baseline performance. The first 1024-actuator DM was integrated in October 2003.

1. Baseline System Characterization

The testbed mirror surface figures were tested with a Zygo interferometer prior to integration. These measurements were used both as a check of the mirror quality as well as an input to our models. The testbed optics were aligned using an interferometer to minimize wavefront error, balancing alignment against some surface errors and yielding an end-to-end wavefront error of 10 nm rms. A flat mirror was used in place of the DM for the alignment, as well as for end-to-end system characterization.

Extensive studies were made using this "baseline" configuration. Wavefront sensing repeatability was investigated, showing a highly stable measurement.¹¹ The repeatability was $\lambda/10,000$ rms over a period of two days for those spatial frequencies controllable by the DM. (Higher spatial frequencies scatter light outside the dark hole and only indirectly impact our contrast as stray light.) Contrast measurements were also performed. The average contrast was 5×10^{-5} at an angular separation of $4 \lambda/D$ and a wavelength of 800 nm. Contrast was 2×10^{-6} at $10 \lambda/D$ and approached 2×10^{-7} at angles exceeding $25 \lambda/D$.

2. Contrast Measurements

The initial measurement taken using a 1024-actuator DM is shown in Figure 5. The front-end (MGS) approach was used to find a zero phase solution. The average contrast is indicated by the solid line, with the points representing the range of contrast values inside the dark hole at a given field angle. At an angle of $4\lambda/D$, the average contrast is 1.8×10^{-6} . The wavelength was 800 nm, with a 5% passband. A radial Gaussian (rotationally symmetric) occulter was used.

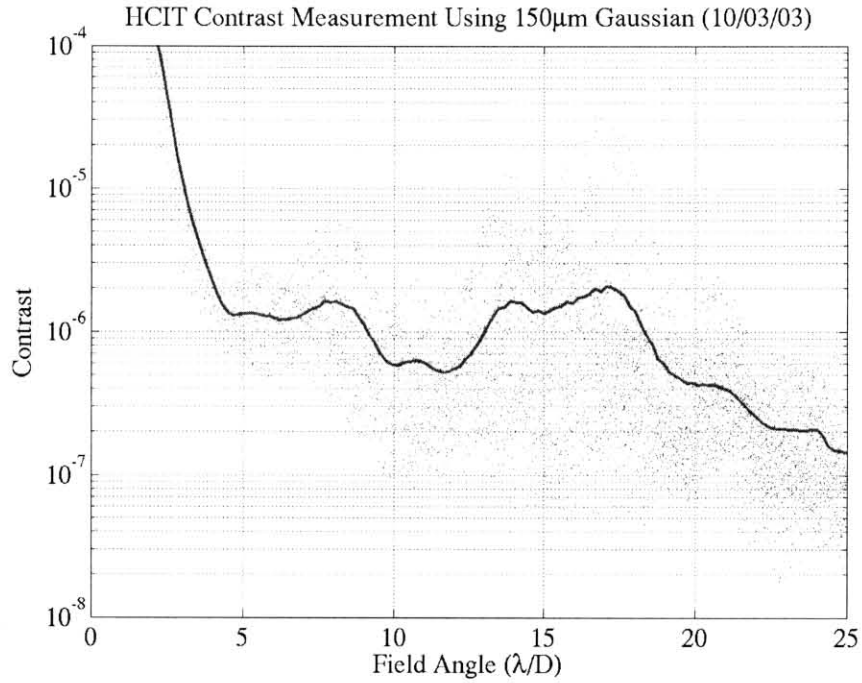


Figure 5. Front-End WFS Contrast Result

Subsequent experiments using a half dark hole algorithm have achieved a dark hole with average contrast better than 5×10^{-9} . To our knowledge, this is the highest contrast ever measured in a laboratory. Figure 6 shows a contrast image, which has the non-occulted image and occulter shape divided out. A 785 nm laser was used with a linear sinc^2 occulter.

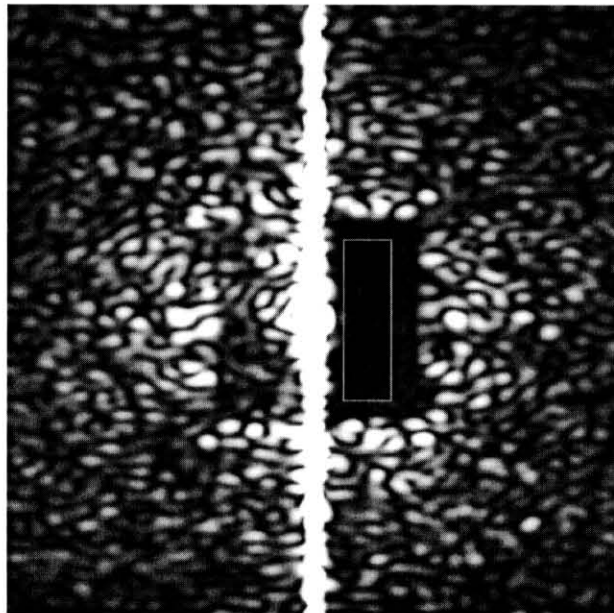


Figure 6. Back-End WFS Contrast Image

The dark hole can easily be moved to the other side of the image. Figures 7a and c show the unnormalized camera images for these cases. Averaging the two solutions gives a full dark hole solution for zero phase (Figure 7b); this is dominated by amplitude errors. A similar solution was found using wavefront sensing at an image of the Lyot (pupil) plane.

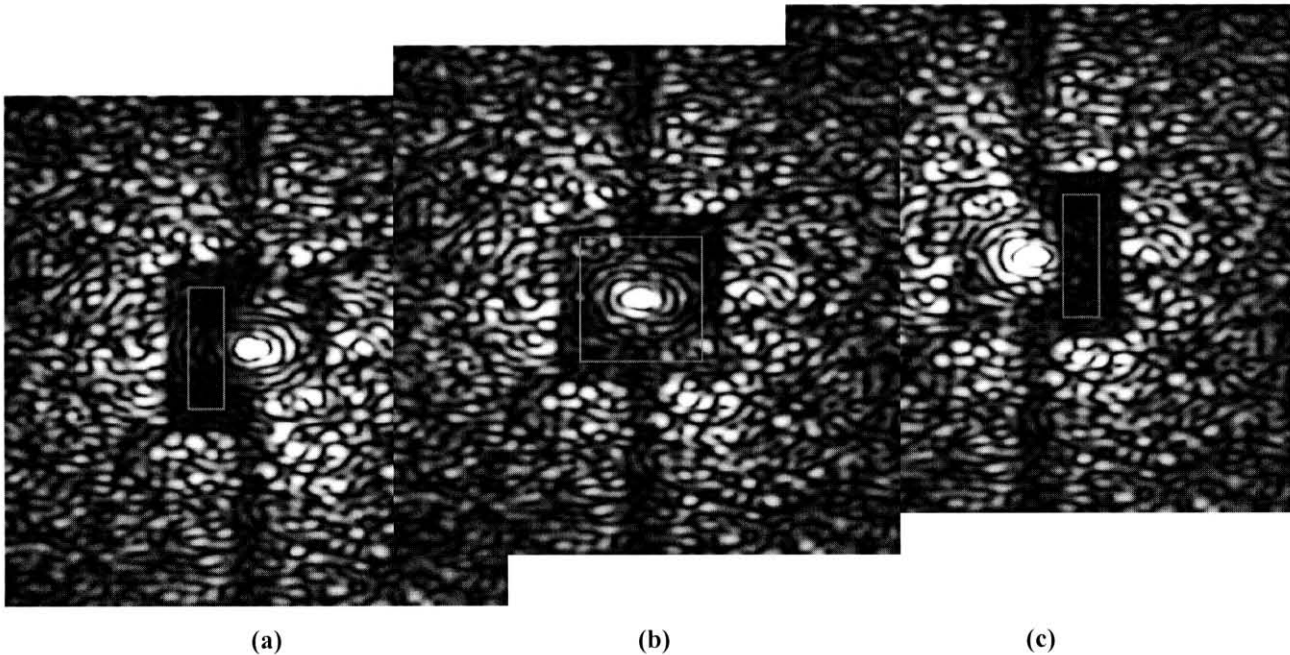


Figure 7. Dark Hole Images: (a) Left Side; (b) Average (Zero Phase); (c) Right Side

5. CONCLUSION

The High Contrast Imaging Testbed provides all the elements needed for demonstration of critical TPF Coronagraph technologies. The testbed environment is highly stable, with demonstrated wavefront sensing repeatability of $\lambda/10,000$. We have measured average contrast of 5×10^{-9} in a half-dark hole using a 1024-actuator deformable mirror; a 4096-actuator mirror will be tested in the near future. Planned refinements in the testbed and improved DMs will push the contrast below 10^{-9} in the next two years. Model and error budget development will demonstrate that these results can be duplicated and will provide a path to the contrast needed in a TPF Coronagraph flight system.

6. ACKNOWLEDGMENTS

The authors wish to thank Bruce Hancock for the MUX ASIC design and Dick Wetzel and Randy Hein for support in hardware design and fabrication at JPL.

Research described in this paper was carried out at the Jet Propulsion Laboratory, California Institute of Technology, under contract with the National Aeronautics and Space Administration.

7. REFERENCES

1. Terrestrial Planet Finder web site, <http://tpf.jpl.nasa.gov>
2. V. G. Ford, A. B. Hull, S. B. Shaklan, M. B. Levine, M. L. White, A. E. Lowman, E. J. Cohen, "Terrestrial Planet Finder Coronagraph," Proc. Soc. Photo-Opt. Instrum. Eng. **5170**, 1-12 (2003).
3. J. T. Trauger, D. Moody, B. Gordon, Y. Gürsel, M. A. Ealey, and R. B. Bagwell, "Performance of a high-density deformable mirror for extremely high contrast imaging astronomy from space," Proc. Soc. Photo-Opt. Instrum. Eng. **4854**, 1-8 (2003).
4. D. C. Redding, S. A. Basinger, A. E. Lowman, A. Kissil, P. Y. Bely, R. Burg, R. G. Lyon, G. E. Mosier, M. Femiano, M. E. Wilson, R. G. Schunk, L. Craig, D. N. Jacobson, J. Rakoczy, J. B. Hadaway, "Wavefront sensing and control for a Next Generation Space Telescope" Proc. Soc. Photo-Opt. Instrum. Eng. **3356**, 758-772 (1998).
5. R. W. Gerchberg and W. O. Saxton, "A practical algorithm for the determination of phase from image and diffraction plane pictures," Optik **35**, 237-246 (1972).
6. S. B. Shaklan, D. Moody, and J. J. Green, "Residual wave front estimation in the reimaged Lyot plane for the Eclipse coronagraphic telescope," Proc. Soc. Photo-Opt. Instrum. Eng. **4860**, 229-239 (2003).
7. J. T. Trauger, B. Gordon, J. J. Green, A. B. Hull, A. E. Lowman, D. Moody, A. F. Niessner, F. Shi, D. W. Wilson, C. Burrows, M. Ealey, M. Mulvihill, "Laboratory technology validation for the Eclipse Coronagraphic Telescope," Proc. Soc. Photo-Opt. Instrum. Eng. **5487-65** (Glasgow, 2004).
8. C. W. Bowers, B. E. Woodgate, R. G. Lyon, "A novel method of high accuracy, wavefront phase and amplitude correction for coronagraphy," Proc. Soc. Photo-Opt. Instrum. Eng. **5170**, 292-306 (2003).
9. D. W. Wilson, P. D. Maker, J. T. Trauger, A. B. Hull, "Eclipse apodization: realization of occulting spots and Lyot masks," Proc. Soc. Photo-Opt. Instrum. Eng. **4860**, 361-370 (2003).
10. R. J. Vanderbei, N. J. Kasdin, D. N. Spergel, M. Kuchner, "New pupil masks for high-contrast imaging," Proc. Soc. Photo-Opt. Instrum. Eng. **5170**, 49-56 (2003).
11. J. J. Green, S. A. Basinger, D. Cohen, A. F. Niessner, D. C. Redding, S. B. Shaklan, J. T. Trauger, "Demonstration of extreme wavefront sensing performance on the TPF high contrast imaging testbed," Proc. Soc. Photo-Opt. Instrum. Eng. **5170**, 38-48 (2003).